Analytical estimation of the key performance points of the tensile force-displacement response of Crescent Shaped Braces

Published Version:
Palermo M., Laghi V., Gasparini G., Silvestri S., Trombetti T. (2021). Analytical estimation of the key performance points of the tensile force-displacement response of Crescent Shaped Braces. SOIL DYNAMICS AND EARTHQUAKE ENGINEERING, 148, 1-4 [10.1016/j.soildyn.2021.106839].

Availability:
This version is available at: https://hdl.handle.net/11585/828808 since: 2024-03-20

Published:
DOI: http://doi.org/10.1016/j.soildyn.2021.106839

Michele Palermo, Vittoria Laghi, Giada Gasparini, Stefano Silvestri, Tomaso Trombetti

Analytical estimation of the key performance points of the tensile force-displacement response of Crescent Shaped Braces

In: Soil Dynamics and Earthquake Engineering, Volume 148, 2021

https://doi.org/10.1016/j.soildyn.2021.106839

Analytical estimation of the key performance points of the tensile force-displacement response of Crescent Shaped Braces

Ph.D Michele Palermo (1), Vittoria Laghi*(2), Ph.D Giada Gasparini (3), Ph.D Stefano Silvestri (4), Ph.D Tomaso Trombetti (5)

Abstract

The technical note investigates the tensile force-displacement response of the hysteretic steel yielding brace known as Crescent Shaped Brace, and characterized by a boomerang-like geometrical shape. The force-displacement curve is governed by three key performance points which correspond to the transition points separating the initial elastic behaviour, the flexural plastic behaviour, the geometrical hardening behaviour and the final axial plastic behaviour.
In particular, the influence of the main geometrical parameter of the device, the so-called "lever arm", on the strongly non-linear force-displacement behavior is analyzed by means of a simplified kinematic model. Based on this, analytical estimations of the key performance points are derived and compared with the numerically simulated force-displacement curves.

Key words

Crescent Shaped Braces; force-displacement response; geometrical non-linearity; mechanical non-linearity; transition lever arm; key performance points; analytical formulas.

1. Introduction

Yielding steel devices are widely used to brace steel structures [1-11]. Among many other solutions presented in the last 40 years, the Crescent Shaped Braces (CSBs) are characterized by a highly non-linear and asymmetric force-displacement *F-u* response (as depicted in Figure 1 of [12]) due to their boomerang-like geometrical shape, mainly characterized by the so-called "lever arm". The mechanical-geometrical coupled nature of the tensile force-displacement response of the CSBs leads to a complex energy dissipation mechanism due to the formation of axial-flexural hinges at the knee-point cross-section [13-17] followed by geometrical hardening and a final axial plastic response.
The first studies on CSBs trace back to the work by Trombetti et al. 2009 [13] which introduced the main feature of a CSB device. Thanks to its original geometrical shape, it is characterized by an initial lateral stiffness which is uncoupled from its lateral yielding strength. This possibility of calibrating the geometrical parameters to obtain selected target responses and the above-mentioned particular *F-u* behavior make the CSB suitable as the base component of a lateral-resisting system capable of achieving multiple performance objectives within the Performance Based Seismic Design framework [18].
Analytical studies were carried out to characterize the response up to the first flexural yielding, followed by numerical studies and by a first series of pseudo-static cyclic tests on small scale (1:6) steel CSB devices [16] aimed at characterizing their cyclic non-linear behavior. More recently, a series of experimental quasi-static cyclic tests on a half-scaled single-bay two-storey frame braced with CSBs were also carried out [17].
In this technical note the role of the lever arm in the force-displacement response under monotonic tensile force is investigated considering a simplified kinematic model, from which an analytical estimation of three key performance points is derived. The analytical estimations of the key performance points allow to predict the ductility and overstrength of the CSB.

2. The role of the "transition lever arm" on the F-u response in tension

A CSB made by two straight elements (AC and CB) of equal lengths L^*, referred to as "symmetric bilinear CSB" is considered (Figure 1a). The angle θ_0 indicates the initial inclination of each straight segment with respect to the line connecting the two end-points A and B (namely, the horizontal direction in Figure 1a). Point A is fixed, while point B is free to move along the lateral direction (u indicates the horizontal displacement along the line connecting the two points A and B). The two end supports do not provide any rotational restraint. One of the main geometrical features of the brace is the "initial lever arm" d_0, namely the vertical distance between the axis connecting A to B (whose length is referred to as $2L_0$) and point C. When the arm d_0 is normalized with respect to the length $2L_0$, it is referred to as $\xi_0=d_0/2L_0$ (subscript *0* refers to the undeformed configuration). When subjected to a lateral force F, the two straight elements of the CSB deform (thick dotted line of Figure 1a) due to the interaction of axial force (compression or tension, depending on the direction of F) and bending moment. The angle between the horizontal direction and the chord of one CSB segment in the generic deformed configuration is indicated with θ and the corresponding lever arm is indicated with d (its normalized value is equal to $\xi=d/2L_0$). The vertical displacement of point C is indicated with v.
The geometrical and mechanical properties of a "symmetric bilinear CSB" are as follows:

- L^* is the length of each straight element;
- L_0 is the projection of L^* in the horizontal plane;
- $\xi_0 = d_0 / 2L_0$ is the normalized initial lever arm;

- h, A and J are the cross-section height, cross-section area and moment of inertia (in-plane), respectively;
- i is the radius of gyration;
- W_e is the elastic section modulus of the cross-section;
- β is the shape factor of the cross-section;
- E is the material Young modulus;
- f_y, ε_y are the yielding strength and strain;
- f_u, ε_u are the ultimate strength and strain;
- r is the hardening ratio.

The influence of the geometrical second-order effects on the force-displacement curve can be evaluated by analyzing the kinematic behavior of the equivalent rigid system, e.g. a system made of two rigid straight segments pinned at the knee point C and having the same global geometry as of the CSB. The kinematic behavior of such system is described by a single degree of freedom, for instance the angle θ that relates the two displacement components u and v:

$$\begin{aligned} u &= 2L^*\left(\cos\theta - \cos\theta_0\right) \\ v &= L^*\left(\sin\theta_0 - \sin\theta\right) \end{aligned} \quad (1)$$

The incremental displacements dv and du are related to ξ_0 by the following analytical expression:

$$\frac{dv}{du}(\theta_0) = \frac{1}{2}\tan^{-1}\theta_0 = \frac{1}{4\cdot\xi_0} \quad (2)$$

Figure 1b displays the trend of dv/du with respect to the normalized initial arm ξ_0. The second-order effects cannot be ignored when the incremental displacement dv becomes much larger than the corresponding incremental displacement du. This condition occurs when $dv/du >> 1.0$. For practical purposes, a value of $dv/du = 5$ can be assumed as the "transition" value. From Figure 1b it can be noted that this transition (e.g. dv/du =5) occurs for a lever arm roughly equal to 5%. Such value of the lever arm can be referred to as the "transition lever arm".

The qualitative graphical representations of the F-u curve of a CSB subjected to tension is shown in Figure 1c. The F-u curve is made by: (i) a first elastic range (governed mainly by the flexural stiffness) until the first *flexural yielding* of the knee-point C is achieved (first key performance point P_{fy}); (ii) a pseudo-plastic plateau region, governed by plasticity and flexural stiffness, that ends at the transition point (second key performance point P_{gh}) with the sudden increase in stiffness due to significant non-linear *geometrical hardening* effects (reduction of the arm d) determining the engagement of the axial stiffness; (iii) a geometric hardening region that ends at P_{ay} (third key performance point) when the brace experiences *axial yielding* while reaching the straight configuration (e.g. the arm d reduces to zero, ξ=0); (iv) a final plastic axial region.

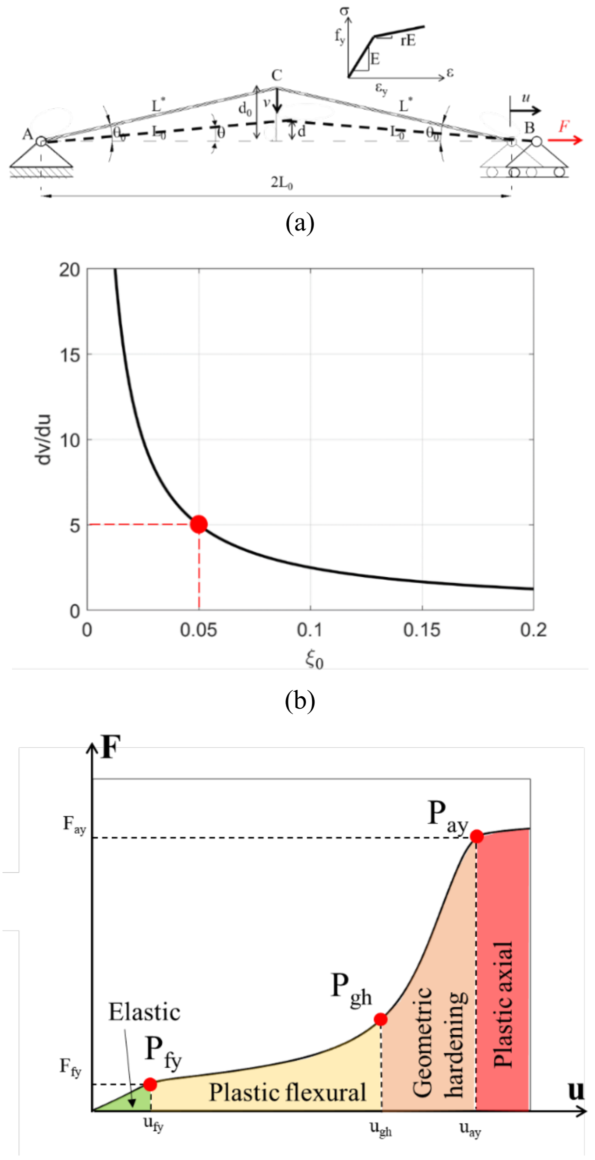

Figure 1*: (a) The "symmetric bilinear" configuration of a CSB subjected to a lateral force F (adapted from [16]). (b) dv/du vs ξ0. (c) The qualitative F-u curve of a CSB with indication of the key performance points.*

3. An analytical estimation of the key performance points of CSBs

The initial elastic behavior of the CSB can be described in terms of the initial lateral stiffness and the flexural yielding force (corresponding to the first performance point) as evaluated imposing the equilibrium in the undeformed configuration [12, 16]:

$$F_{fy} = \frac{W_e \cdot f_y}{d_0}\cdot\gamma = \frac{f_y \cdot J}{L_0 \cdot h \cdot \xi_0}\cdot\gamma \quad (3)$$

$$u_{fy} = \frac{8}{3}\cdot\frac{f_y \cdot L_0^{\,2}\cdot\xi_0}{E\cdot h\cdot\cos\theta_0}\cdot\gamma \quad (4)$$

$$k_{IN} = \frac{3}{8}\cdot\frac{E\cdot J\cdot\cos\theta_0}{L_0^{\,3}\cdot\xi_0^{\,2}} \quad (5)$$

$$\gamma = \frac{1}{1 + \frac{h}{2L_0} \cdot \frac{2}{\xi_0} \cdot \left(\frac{i}{h}\right)^2} \qquad (6)$$

where γ is a reduction factor ($\gamma \leq 1.0$) depending on the axial force - bending moment interaction.

From Eq. 1, the lateral displacement u_{gh} (second performance point P_{gh} corresponding to the ξ=5% configuration) results equal to:

$$u_{gh} = 2L_0 \frac{\left|\left(\cos\theta_{5\%} - \cos\theta_0\right)\right|}{\cos\theta_0} \qquad (7)$$

where $\theta_{5\%}$ indicates the angle corresponding to the configuration with ξ=5%.

The ratio u_{gh}/u_{fy} can be considered as a measure of the displacement ductility in tension:

$$\mu_t = \frac{3}{4}\frac{E}{f_y}\frac{h}{L_0}\frac{\left|\left(\cos\theta_{5\%} - \cos\theta_0\right)\right|}{\xi_0 \cdot \gamma} \qquad (8)$$

Eq. 8 clearly highlights that the ductility of the CSB depends on the product of three main factors: a factor related to the material mechanical properties (E/f_y), a slenderness parameter ($h/2L_0$) and a function $f(\xi_0) = \left|\left(\cos\theta_{5\%} - \cos\theta_0\right)\right| / (\xi_0 \cdot \gamma)$ dependent on the "distance" between the initial geometrical configuration and the configuration characterized by ξ=5%.

The axial yielding force F_{ay} corresponding to the third performance point P_{ay} can be evaluated as:

$$F_{ay} = A \cdot f_y \qquad (9)$$

The displacement u_{ay} at point P_{ay} can be estimated as the sum of the contributions due to the rigid body rotation (Eq. 1) and the elastic deformation ε_y (just before yielding point due to axial tension):

$$u_{ay} = \frac{2L_0}{\cos\theta_0}\left(1 - \cos\theta_0 + \varepsilon_y\right) \qquad (10)$$

The ratio between F_{ay} and F_{fy} can be interpreted as an over-strength factor Ω:

$$\Omega = \frac{L_0 \cdot h}{i^2}\frac{\xi_0}{\gamma} \qquad (11)$$

4. Comparisons with the results of non-linear simulations

The level of approximation in the estimation of the key performance points of the *F-u* curves according to the proposed analytical equations (Eqs. 1-11) can be appreciated through comparison with the full *F-u* response obtained from numerical simulations developed with the Finite Element software SeismoStruct [19]. A CSB device with total horizontal length ($2L_0$) equal to 300 cm and full squared cross-section (10 cm x 10 cm) has been analyzed. Each straight segment of the CSB is modelled with four beam elements using the force-based formulation [20]. Non-linear geometry is approached using the corotational formulation [21]. Material non-linearity is accounted using an elasto-plastic constitutive model with isotropic hardening (hardening ratio r=0.005). Material Young's modulus is set equal to E=210000 MPa and the yielding strength is f_y=355 MPa. The ultimate strain is set equal to ε_u =0.3.

Figure 2 compares the analytical piece-wise linear curves (red dashed lines) obtained by simply connecting the three performance points (red dots) P_{fy}, P_{gh} (the force at point P_{gh} is set equal to F_{fy}) and P_{ax} (as computed according to the analytical formulas derived in the previous section) and the numerical *F-u* curves of three CSBs with different d_0 values (30 cm, 45 cm and 60 cm, corresponding to ξ_0 values equal to 10%, 15%, and 20%, respectively). The graphs clearly show that the analytical equations are able to capture the main features of the whole non-linear behavior in tension.

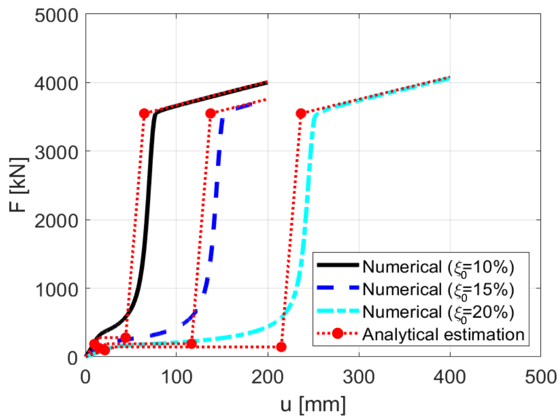

***Figure 2**: Comparison between numerical F-u curves and analytical estimation of the key performance points.*

It is worth noticing that the shift in the geometrical hardening phase between the analytical and numerical curves is related to the assumed simplified kinematic model (Eq. 1, Figure 1a) which neglects the axial deformation of the CSB. Such approximation appears reasonable for initial lever arms values between 5% and 20%.

It should be noted that the aim of the analytical formulas is not to accurately capture the whole non-linear response, rather to provide practical tools useful for the preliminary design of CSB devices.

5. Conclusions.

This study provides new insights into the non-linear behavior of a steel yielding brace called Crescent Shaped Brace (CSB), which is governed by a strong interaction between geometrical and mechanical non-linearities. The attention has been paid to the tensile post-yielding force-displacement response. It is found that the final geometric hardening behavior (related to the engagement of the axial stiffness due to significant non-linear geometrical effects) experienced under tensile forces after the pseudo-plastic plateau is triggered by a "transition lever arm" corresponding to a normalized value of 5%. This finding indicates that the initial lever arm has to be carefully chosen in order to ensure the required level of ductility under tensile loads. The force-displacement curve of the CSB in tension is analytically derived through the definition of three key performance points, defining different phases of the CSB behavior: (i) elastic phase, (ii) plastic flexural phase, (iii) geometric hardening phase and (iv) final plastic axial phase. The validity of the analytical estimations is verified through numerical simulations. The results confirm that the proposed formulas provide a good level of approximation of the overall force-displacement behavior of the CSB for preliminary design purposes.

References

[1] Skinner RI, Kelly JM, Heine AJ. Hysteretic dampers for earthquake-resistant structures. Earthq Eng Struct Dyn 1974;3:287–96.

[2] Tyler RG. Tapered Steel Energy Dissipators for Earthquake Resistant Structures. Bull New Zeal Natl Soc Earthq Eng 1978;11:282–94.

[3] Whittaker A, Bertero VV, Alonso J, Thompson C. Earthquake Simulator Testing of Steel Plate Added Damping and Stiffness Elements. 1989. https://doi.org/10.13140/RG.2.1.1455.3207.

[4] Tsai K-C, Chen H-W, Hong C-P, Su Y-F. Design of Steel Triangular Plate Energy Absorbers for Seismic-Resistant Construction. Earthq Spectra 1993;9:505–28. https://doi.org/10.1193/1.1585727.

[5] Garivani S, Aghakouchak AA, Shahbeyk S. Numerical and experimental study of comb-teeth metallic yielding dampers. Int J Steel Struct 2016;16:177–96. https://doi.org/10.1007/s13296-016-3014-z.

[6] Kato S, Kim YB, Nakazawa S, Ohya T. Simulation of the cyclic behavior of J-shaped steel hysteresis devices and study on the efficiency for reducing earthquake responses of space structures. J Constr Steel Res 2005. https://doi.org/10.1016/j.jcsr.2005.03.006.

[7] Pujari NN. Optimum Placement of X-Plate Dampers for Seismic Response Control of Multistoried Buildings. October 2011;04:481–5.

[8] Baiguera M, Vasdravellis G, Karavasilis TL. Dual seismic-resistant steel frame with high post-yield stiffness energy-dissipative braces for residual drift reduction. J Constr Steel Res 2016;122:198–212.

[9] Gray MG, Christopoulos C, Packer JA. Cast steel yielding brace system for concentrically braced frames: concept development and experimental validations. J Struct Eng 2014;140:4013095.

[10] Hsu H-L, Halim H. Improving seismic performance of framed structures with steel curved dampers. Eng Struct 2017;130:99–111.

[11] Jia L-J, Ge H, Maruyama R, Shinohara K. Development of a novel high-performance all-steel fish-bone shaped buckling-restrained brace. Eng Struct 2017;138:105–19. https://doi.org/10.2174/1874836800903020127.

[12] Palermo M, Silvestri S, Gasparini G, Trombetti T. Crescent shaped braces for the seismic design of building structures. Mater Struct 2015;48:1485–502. https://doi.org/10.1617/s11527-014-0249-z.

[13] Trombetti T, Silvestri S, Gasparini G, Ricci I. Stiffness-Strength-Ductility-Design Approaches for Crescent Shaped Braces. Open Constr Build Technol J 2009;3:127–40.

[14] Palermo M, Ricci I, Gagliardi S, Silvestri S, Trombetti T, Gasparini G. Multi-performance seismic design through an enhanced first-storey isolation system. Eng Struct 2014. https://doi.org/10.1016/j.engstruct.2013.11.002.

[15] Kammouh O, Silvestri S, Palermo M, Cimellaro GP. Performance-based seismic design of multistory frame structures equipped with crescent-shaped brace. Struct Control Heal Monit 2018;25:1–17. https://doi.org/10.1002/stc.2079.

[16] Palermo M, Pieraccini L, Dib A, Silvestri S, Trombetti T. Experimental tests on Crescent Shaped Braces hysteretic devices. Eng Struct 2017;144:185–200. https://doi.org/10.1016/j.engstruct.2017.04.034.

[17] Mokhtari E, Laghi V, Palermo M, Silvestri S. Quasi-static cyclic tests on a half-scaled two-storey steel frame equipped with Crescent Shaped Braces. Eng Struct 2021;232. https://doi.org/10.1016/j.engstruct.2020.111836.

[18] Bertero RD, Bertero V V. Performance-based seismic engineering: The need for a reliable conceptual comprehensive approach. Earthq Eng Struct Dyn 2002;31:627–52. https://doi.org/10.1002/eqe.146

[19] SoftwareSolutions SEE. SeismoStruct n.d. http://www.seismosoft.com/en/HomePage.aspx.

[20] Spacone E, Ciampi V, Filippou FC. Mixed formulation of nonlinear beam finite element. Comput Struct 1996. https://doi.org/10.1016/0045-7949(95)00103-N.

[21] Correia AA, Virtuoso FBE. Nonlinear analysis of space frames. 3rd Eur. Conf. Comput. Mech. Solids, Struct. Coupled Probl. Eng., Lisbon, Portugal: 2006.